Available online at www.sciencedirect.com
ScienceDirect
Catalysis Today 130 (2008) 309–319
CATALYSIS TODAY
www.elsevier.com/locate/cattod

Synthesis, characterization and catalytic properties of NiMo/Al_2O_3–MCM-41 catalyst for dibenzothiophene hydrodesulfurization

R. Silva-Rodrigo [a,*], F. Hernández-López [a], K. Martinez-Juarez [a], A. Castillo-Mares [a], J.A. Melo Banda [a], A. Olivas-Sarabia [b], J. Ancheyta [c], M.S. Rana [c]

[a] *Instituto Tecnológico de Cd. Madero, División de Estudios de Posgrado e Investigación, Juventino Rosas y Jesús Urueta S/N, Col. Los Mangos, Cd. Madero, Tamps 89440, Mexico*
[b] *Centro de Ciencias de la Materia Condensada, UNAM, A.P. 2681 Ensenada, B.C. 22800, Mexico*
[c] *Instituto Mexicano del Petróleo, Eje Central Lázaro Cárdenas No. 152, Distrito Federal 07730, Mexico*

Available online 28 November 2007

Abstract

Ni–Mo/Al_2O_3–MCM-41 supported catalysts have been investigated for modification of MCM-41 by using sol–gel alumina incorporation method. Different catalysts were synthesized with variation of Si/Al molar ratios of 10, 50, 100 and 200. High specific surface area ordered meso-porous solid (MCM-41) was synthesized by using organic template method. In order to modify the low acidity of silica solid, the surface of MCM-41 was modified by incorporation of alumina. The surface acidity of solids modified significantly with variation of alumina content in the supports. The sol–gel method of alumina incorporation was used, which does not modify extensively the pore characteristics of MCM-41 material during the preparation of Al_2O_3–MCM-41. The X-ray diffraction intensities indicated that alumina as well as MCM-41 were present in the synthesized supports. Additionally, the hydrothermal stability of the Al_2O_3–MCM-41 materials was maintained up to 873 K using sever conditions like 100% water vapor stream. The catalytic activity of the catalysts was tested in the hydrodesulfurization (HDS) of dibenzothiophene (DBT). Selectivity was oriented mainly to the production of biphenyl (BP) and for high Si/Al ratios toward cyclohexylbenzene (CHB) and showed a higher conversion and better selectivity to hydrogenation (cyclohexylbenzene).

Keywords: Hydrodesulfurization; Sol–gel γ-Al_2O_3; Meso-porous NiMo/Al_2O_3–MCM-41 catalysts; NH_3-TPD

1. Introduction

Petroleum refining industries are the major input to generate the power requirements of the changing world, and the combustion of petroleum hydrocarbons is well known as anti-environment effects. Thus, the environmental regulations are stricter on the legislation of green effects, which are mainly effected due to the emissions of sulfur and nitrogen compounds (SO_x, NO_x). To the search of clean fuel, countries like Japan, USA and the European Union are a measure to control these emissions, since the have united their forces stipulating maximum permissible sulfur level in petroleum fuels near or lower than 50 ppm [1]. To remove S and N organic species from the different petroleum fractions catalytic hydrotreating processes require the use of effective catalysts to accomplish the regulations and favor the least corrosive compounds emissions to the environment [2]. It has also been demonstrated that among the most difficult organic sulfur molecules are DBT or its substitutes compounds such as 4,6-dimethyl-dibenzothiophene. To remove these complex sulfur molecules in the feedstock an acidic supported catalyst along with high surface area is needed to promote the HDS of complex molecules. In this sense, at the beginning of 1990, Mobil Oil Company developed the M41S family materials, which possess regular meso-porous system and high surface areas near to 1000 m^2/g

* Corresponding author. Tel.: +52 8332158544; fax: +52 8332158544.
E-mail addresses: rebsilva_2000@yahoo.com.mx (R. Silva-Rodrigo), jancheyt@imp.mx (J. Ancheyta).

0920-5861/$ – see front matter © 2007 Elsevier B.V. All rights reserved.
doi:10.1016/j.cattod.2007.10.001

[3,4]. Nickel and molybdenum supported on alumina catalysts are limited by their medium or low surface area, but have excellent stability at industrial practice. Moreover, a small pore size material decreases its application for complex molecules or heavy oils.

The present work deals with catalytic supports like MCM-41 modified with alumina added during the synthesis of the mesoporous materials, with the purpose of taking advantage of their attractive properties such as high surface area, large pore volume, defined pore structure and favorable acidity. The method of alumina incorporation used sol–gel technique, since it is able to create materials with high thermal stability, homogeneity, purity of the materials and high defined pore distribution. The prepared materials, MCM-41 and γ-Al_2O_3, presented a series of different Si/Al ratios starting with 10, 50, 100 and 200 being later impregnated with Ni and Mo as active metallic phases, and finally used for the HDS reaction of dibenzothiophene.

2. Experimental

The MCM-41 materials were prepared by following a conventional method described by Terrés and co-workers [5]. Cetyltrimethyl ammonium bromide (CTAB) ($C_{19}H_{42}NBr$; Aldrich, 99%) was a tenso-active material which together with ammonium hydroxide (NH_4OH) was added to deionized water at room temperature. Both were previously weighted according to the molar ratio (CTAB/TEOS = 4.08 and CTAB/NH_4OH = 0.21) used for synthesis, the mixture was stirred from 20 to 45 min, later tetraethyl orthosilicate (TEOS) ($C_8H_{20}O_4Si$; Aldrich 99.9%) was added to the mixture as a source of silica. The introduction of alumina into MCM-41 was during the synthesis of the MCM-41 "*in situ*" just before NH_4OH was added, to obtain a supports AM(x) (Al_2O_3–MCM-41) series, where x is the Si/Al molar ratio (Si/Al = 10, 50, 100 and 200). Once stirring was completed, the mixture was filtered, and the supports were dried at 343 K and calcined at 813 K in presence of air. Table 1 presents the molar compositions used for preparation of support along with the Si/Al ratio of the supports. The pure sol–gel (Al_2O_3-SG) alumina support was prepared by mixing aluminium tri-sec-butoxide [$Al(OC_4H_{9sec})_3$] (0.207 mL), in 6.5 mol of absolute ethanol a 333 K. Reactants were maintained under constant stirring and refluxing. Distilled water (2.94 mol) was added to the mixture and the gelling reaction was completed. Thereafter, the gel was dried in air at 343 K for 24 h (fresh samples) [6]. Materials were calcined at 873 K, 1 h in nitrogen atmosphere and 6 h in air in order to obtain gamma phase of alumina.

Table 1
Molar compositions of the supports

Supports	Si/Al	Molar composition			
		CTAB	NH_4OH	TEOS	Al_2O_3 SG
MCM-41	–	0.2	0.92	0.049	–
AM10	10	0.2	0.92	0.049	6.15
AM50	50	0.2	0.92	0.049	1.23
AM100	100	0.2	0.92	0.049	0.62
AM200	200	0.2	0.92	0.049	0.30

AM: (Al_2O_3 + MCM-41); SG: sol–gel alumina.

Table 2
Catalysts composition

Catalysts	Composition (wt.%)			
	Si/Al	Mo	Ni	Ni/(Ni + Mo)
CAM10	10	17.12	5.26	0.33
CAM50	50	17.78	5.47	0.33
CAM100	100	15.73	4.84	0.33
CAM200	200	17.98	4.84	0.31
CM41	–	17.38	5.5	0.34

The catalysts were prepared by means of simultaneously impregnation of ammonium heptamolybdate and nickel nitrate with a Ni/(Ni + Mo) ratio of 0.3, which is typical of the metals composition for industrial catalysts. The composition of NiMo catalysts is given in Table 2.

The structural properties of the catalysts were characterized by X-ray diffraction using a Bruker AXS diffractometer (model 8000), using the Cu Kα radiation and scanning at 0.6° min^{-1}, within the range of $1.5 < 2\theta < 10$ and $10 < 2\theta < 80$.

Textural properties of the supports were determined by N_2 adsorption at 78 K, using Quantachrome AUTOSORB-1 sorptometer. Surface area was calculated from the BET equation, while pore and average pore diameters were obtained from the desorption isotherm using the BJH method. Before the BET measurements, the samples were pretreated at 623 K for 2 h.

Acid sites distribution was determined by thermal programmed desorption (TPD) (*in situ*) of NH_3 using a RIG-100-19 system fitted with a thermal conductivity detector (TCD). The samples were pretreated at 723 K, 2 h in helium atmosphere, before ammonia adsorption at 473 K. Thermal desorption was scanned within the range from 373 to 873 K, while the classification of the acid sites distribution was determined following the procedures reported elsewhere [7–9].

The study of functional groups of the supports was made by means of infrared spectroscopy (conventional transmittance) with a Perkin-Elmer apparatus (Paragon 2000) in which wafers were prepared with KBr.

The hydrothermal stability of the catalysts was tested using a quartz reactor with water vapor flow (with an air flow of 100 mL/min) at 673, 773 and 873 K, for 2 h, at a heating rate of 2 K/min.

Wall-thickness for various materials was calculated from the difference between lattice parameter (hexagonal array) and pore diameter [10]:

$$\delta = \alpha_0 - D_{ps} \quad (1)$$

$$\alpha_0 = \frac{2d_{100}}{\sqrt{3}} \quad (2)$$

where α_0 is the cell parameter (hexagonal array) (Å); d_{100} the inter-planar distance (from Scherrer's equation); $d = (\lambda/2)\sin(\theta)$; λ the X-rays wavelength (Å); θ the diffraction angle;

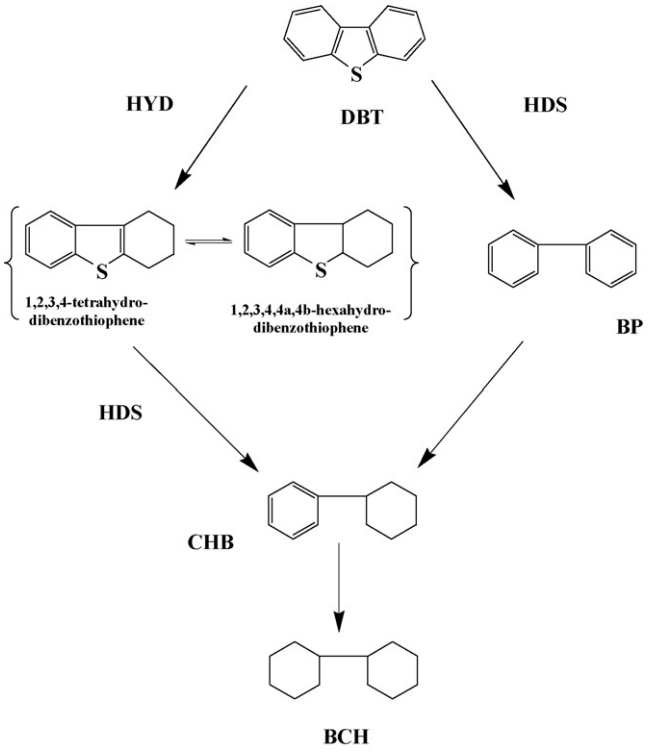

Fig. 1. Dibenzothiophene reaction network [13].

δ the wall-thickness (Å); D_{ps} is the pore diameter (from BJH calculations, adsorption data, N_2 physisorption isotherm) (Å).

DBT hydrodesulfurization was chosen as the catalytic activity test. The dibenzothiophene HDS reaction scheme is shown in Fig. 1 [11]. The HDS reaction of DBT involves two alternative pathways. One way involves the cleavage of the C–S bond without cleavage of the aromatic ring producing BP as the main product. A second mechanism is presented with the hydrogenation of one of the aromatic rings, maintaining the heteroatom bonded to the other aromatic ring, tetrahydrodibenzothiophene (THDBT). A hydrogenation produces the CHB, product that will take place when the two reaction mechanisms of HDS of DBT are in the pseudo-stable equilibrium. At the end it is observed the reaction of CHB which will produce bicyclohexyl (BCH) by the hydrogenation way. The production of THDBT and hexahydrodibenzothiophene (HHDBT) varied with the characteristics of the catalyst (hydrogenation capacity) but their presence at the conditions of these experiments was insignificant.

Catalytic activity was determined in a Parr batch reactor with a capacity of 500 mL using 230 mL solution of DBT (0.1 wt.% S), which was dissolved in a mixture of *cis*- (53%) and *trans*-decalin (44%) solvent, and decane (0.05 mol/L) as an internal reference. A catalyst mass (0.88 g) was dried at 673 K for 1 h before loaded to the reactor for each experiment. Prior to the HDS reaction, the catalysts were activated (*ex situ* sulfidation) with a mixture of $H_2 + CS_2$ at 673 K for 3 h in glass reactor. The HDS reaction was carried out at the following operation conditions: reaction temperature of 613 K, pressure of 45 bar, stirring rate of 700 rpm and reaction time of 3 h. The reactant and products were diluted precisely in ethanol (500 μL) and analyzed by GC using a FID detector and a capillary column at a temperature programmed from 40 to 150 °C.

3. Results and discussion

3.1. X-ray diffraction

XRD patterns of calcined supports are shown in Fig. 2, three characteristic intensities can be indexed as a hexagonal lattice of a typical MCM-41 of $d_{1\,0\,0}$, $d_{1\,1\,0}$ and $d_{2\,0\,0}$ for basal space, geometry and periodicity, respectively [12]. The characteristic low angle intensities for MCM-41 such as $2\theta = 2.3^\circ$ was present in all the supports. For the support with Si/Al ratios >50 signals appear in 3.9° and 6° 2θ angle, which suggest a loss of the homogeneity and hexagonal symmetry of the crystalline structure due to an increase in alumina content, however, when using such a high amount of alumina this loss of crystallinity is trivial or rather normal. On the other hand, high 2Θ angle is shown in Fig. 3, in which X-ray diffraction patterns ($2\theta = 40$–70°) are shown for the AM supports that are the MCM-41 modified supports with alumina. To verify the crystal growth due to the incorporated alumina, 46°, 53° and 66° 2θ were indicative of poor crystal formation and the intensities that appear can be indication of small clusters of aluminum that brought from gamma alumina. Therefore, the low and high angle intensities of these MCM-41 and Al_2O_3 materials are indicative to the existence of diverse phases. However, the possibility of Al clusters can have a number of explanations, which can be a matter of further studies, but the present

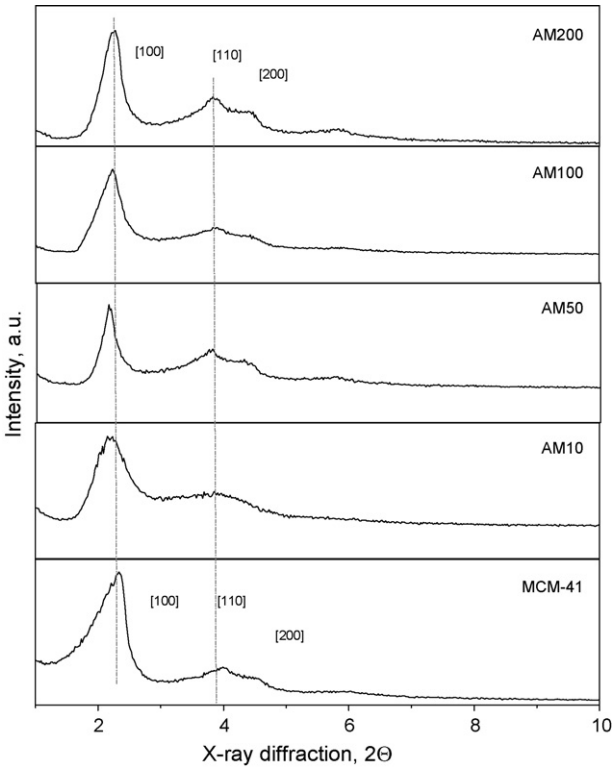

Fig. 2. XRD patterns of Al_2O_3–MCM-41 supports for $2\theta = 0$–10°.

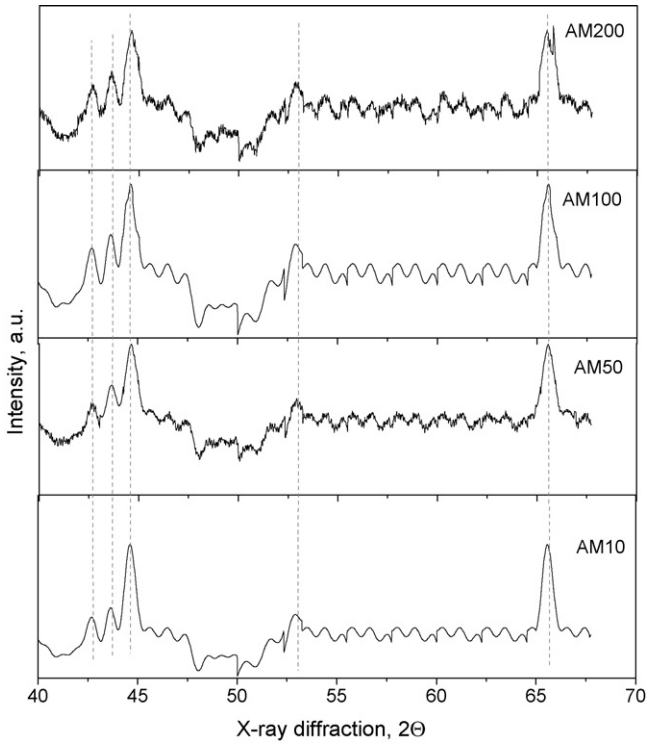

Fig. 3. XRD patterns of Al_2O_3–MCM-41 supports for $2\theta = 40–70^\circ$.

characterization techniques indicated that the alumina is on the surface and not in the form of bulk.

The diffractograms of Ni and Mo supported catalysts are shown in Fig. 4. The metal oxides appear with different interaction with variation of alumina content, the metal oxide species are identified with a standard ASTM data files. The dominating metal oxides are the MoO_3 (ASTM 5-0508) and NiO (ASTM 44-1159). Low molybdenum interaction with surface alumina support is seen in the case of Si/Al = 50, which may indicate that the optimum loading may occur at around this loading of alumina on the MCM-41. Further loading of alumina is easily accessed to the molybdenum active phases and promote the formation of $Al_2(MoO_4)_3$ (ASTM 23-764) species as it is evident in the case of CAM50 and CAM10.

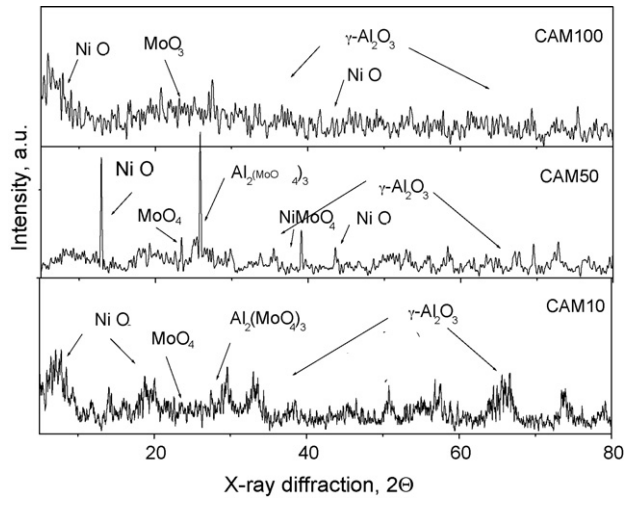

Fig. 4. XRD patterns of the catalysts for $2\theta = 0–80^\circ$.

Table 3
Surface area (SA), pore diameter (D_{ps}) and pore volume (PV) of supports and catalysts

Samples	SA (m^2/g)	D_{ps}[a] (Å)	PV (cc/g)
Supports			
MCM-41	997	53	1.30
AM10	974	50	1.23
AM50	1037	44	1.14
AM100	846	50	1.13
AM200	1058	41	1.19
Al_2O_3SG	215	259	1.40
NiMo catalysts			
CM41	242	95	0.577
CAM10	221	56	0.311
CAM50	198	45	0.211
CAM100	158	30	0.121
CAM200	352	51	0.450

[a] Pore diameter determined from the desorption isotherm by the BJH method.

3.2. Textural properties

The nitrogen physisorption analysis indicated that the addition of alumina had not significant effect on the specific surface area and pore volume of supports as shown in Table 3. The support areas of AM varied within the range of experimental error, observing the meso-porous characteristics of MCM-41, which are not affected with a great extent by addition of the sol–gel alumina. It is reported in the literature that the use of traditional alumina has as disadvantage that the incorporation of Al atoms into the MCM-41 framework causes a diminution of the textural characteristics [13,14], however this does not happen in the case of the AM supports of the present work. Thus, the novelty of this work was the preparation of alumina by the sol–gel method. Additionally, the pore diameter of the Al_2O_3–MCM-41 (AM) supports varied from 41 to 53 Å confirming the intact meso-porous structure of MCM-41 materials.

The textural property results are complementary to the low angle XRD ($2\Theta = 0–10^\circ$) intensities, which does not demonstrate major changes in the hexagonal arrangement of the pore after alumina incorporation. The results of Si/Al ratio, pore diameter and unit cell parameters (α_0) along with the wall-thickness of Al_2O_3–MCM-41 are shown in Table 4. The wall-thickness of MCM-41 increases with increasing the alumina loading, i.e. up to the 28 Å in the case of AM10, which is almost

Table 4
Wall-thickness of the supports

Supports	Si/Al	D_{ps} (Å)	$d_{1\,0\,0}$ (Å)	α_0 (Å)	δ (Å)
MCM-41	–	53	53.56	61.58	8.85
AM10	10	50	68.01	78.53	28.53
AM50	50	44	56.81	65.60	21.60
AM100	100	50	54.12	62.49	12.49
AM200	200	45	49.53	57.02	12.20

δ: wall-thickness; α_0: cell parameter; $d_{1\,0\,0}$: inter-planar distance.

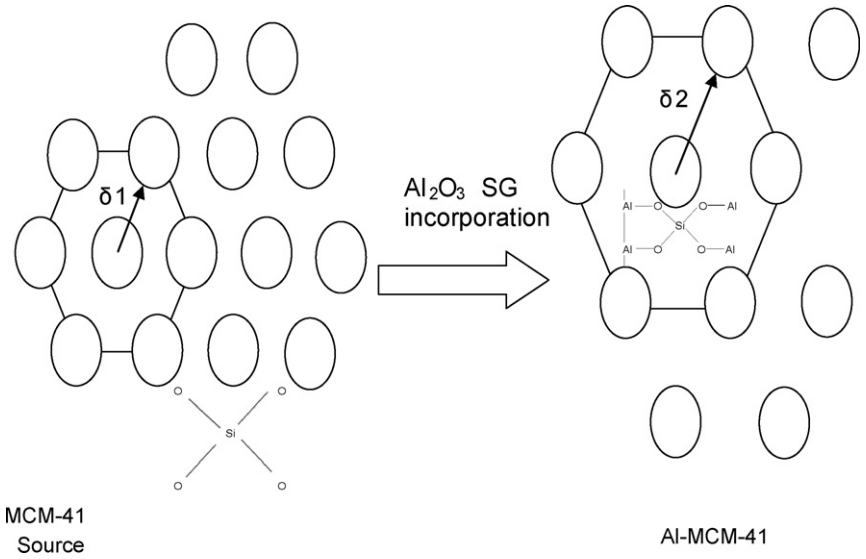

Fig. 5. Hypothetical incorporation of Al into MCM-41 (SiO_2) framework, since the wall-thickness (δ) was increased with Al content.

three times higher than that of MCM-41. This behavior also establishes that the increased wall-thickness is due to the Al–O–Si network formation but maintaining the same average pore diameter of the support. A hypothetical structure of deposited Al and MCM-41 is reported in Fig. 5, which shows the possibility of Al interaction into the siliceous MCM type framework. Also, the characteristic peak of MCM-41 pore source appears at $2\theta = 2.4^\circ$, while for the other supports the same peak ($d_{1\,0\,0}$) was found at $2\theta = 2.25^\circ$. These results ascertain that basal space was changed in the original position with the incorporation of Al in the –Si–O framework (Fig. 2). On the other hand, the textural properties of NiMo supported catalyst decrease significant by 67–81%, indicating that noticeable changes occurred during the catalysts preparation.

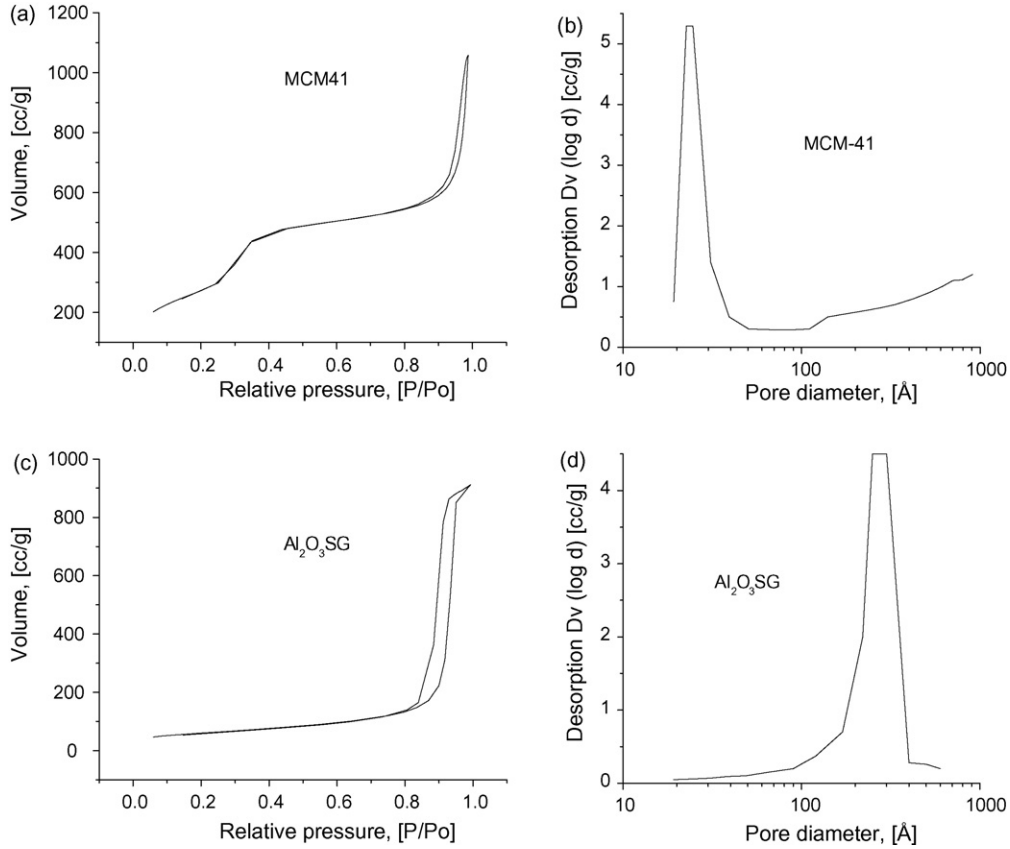

Fig. 6. Isotherms for adsorption–desorption of supports: (a) MCM-41 and (c) Sol–gel alumina and pore size distribution of supports; (b) MCM-41 and (d) Sol–gel alumina.

As can be seen from Table 3, the pore diameter of pure MCM-41 increases by 1.8 times, which further indicated that the during catalyst preparation the stability of MCM-41 is a matter of impregnation pH and the conditions used. The decrease in specific surface area and pore volume could be due to pore blockage, but the pore diameter of these catalysts remain almost the same as in the support, which is not likely due to the pores blockage. Therefore, it is more probable that specific surface area and pore volume decrease due to the stability of siliceous material.

3.2.1. Adsorption–desorption isotherms and pore size distribution

The N_2 adsorption–desorption isotherms represent type IV hysteresis for all the supports corresponding to meso-porous solids as shown in Figs. 6 and 7a. This hysteresis corresponds to aggregates or agglomerates of particles forming slit shaped pores (plates or edged particles like cubes) with uniform distribution [15]. These results are in accordance with the pore size distributions that are fairly homogeneous and unimodal in nature as shown in Figs. 6 and 8.

For the catalysts with Si/Al ratios of 10, 50 and 200, the isotherms did not present a significant variation being type IV with H4 hysteresis (Figs. 7 and 9). These isotherms exhibited a relative high adsorption in the relative pressure range of 0.35–0.45 and that has been reported as a characteristic of capillary condensation in uniform meso-porous. It can also be observed that the incorporation of alumina did not affect the form of the isotherms including Si/Al = 10. On the other hand, NiMo supported catalysts showed significant adsorption–desorption isotherm changes, particularly CAM100 catalyst (Fig. 7b) showed type II isotherms with a H3 hysteresis. This behavior may be attributed to a very high loss of meso-pore structure of the Al_2O_3–MCM-41 which also corresponds to a decrease in the textural properties. Pore distribution for all of the catalysts was mono-modal showing that they belong to the meso-porous oscillating between 30 Å except for CM41 with 95 Å, while CAM100 catalyst showed completely different pore pattern indicating that there is no more meso-pores, which were converted into macro-pores or multi-modal pore distribution (Fig. 10). The textural property results contribute to conclude that the insertion of Al into the MCM-41 using sol–gel method does not change the hexagonal array but during the impregnation of Ni and Mo the structure of MCM-41 is seriously damaged.

3.3. FTIR spectroscopy

Fig. 11 shows the IR spectra of the supports, where the presence of Al–O–Al fundamental bond vibration of alumina was observed for Al_2O_3–MCM-41 supports. The band appears around 1000 cm^{-1} and it confirms that the aluminum source was incorporated during the synthesis. However, there is no clear or very low evidence for the presence of 960 cm^{-1} band for Al–O–Si band characteristic, which appears to decrease with increasing Al content. The characteristic bands of MCM-41 type material appear at about 2320, 1220–1010, 800 and

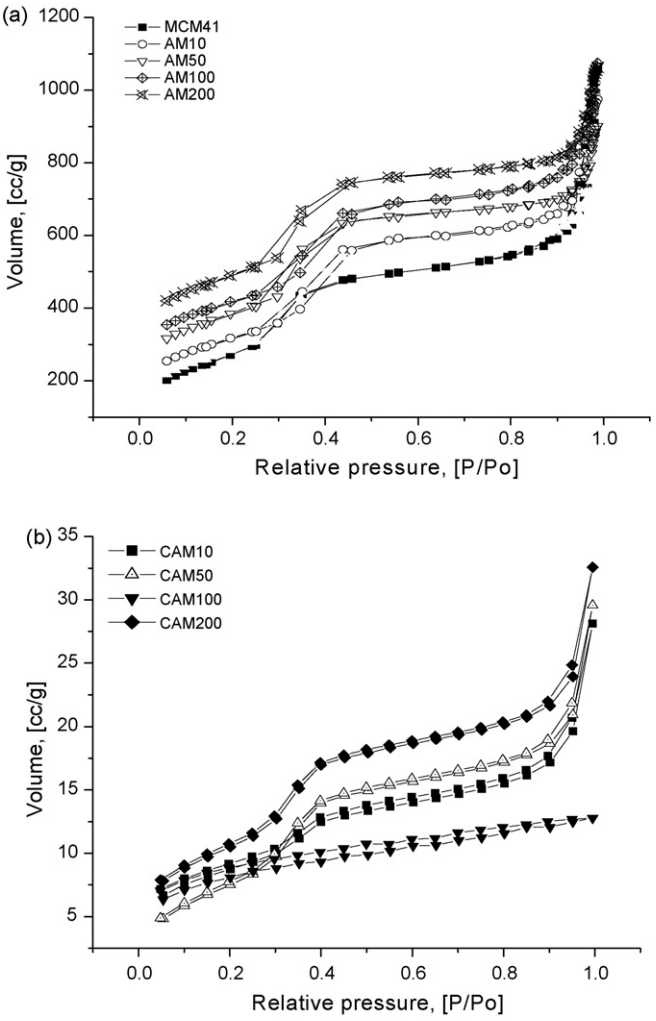

Fig. 7. Isotherms of adsorption–desorption: (a) supports and (b) catalysts.

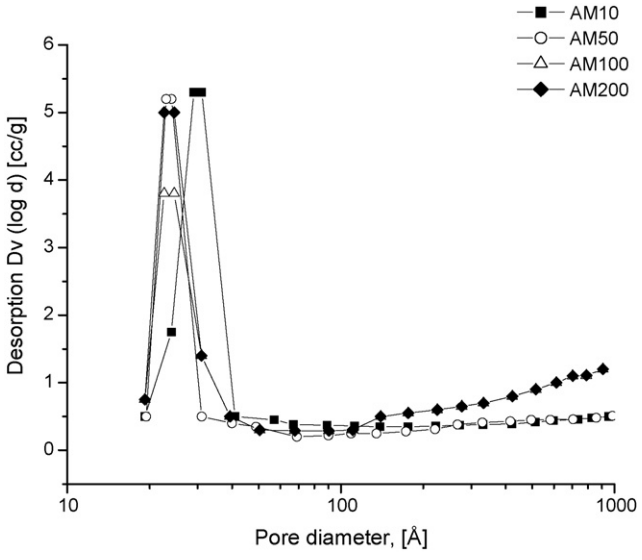

Fig. 8. Pore size distribution of supports: AM10, AM50, AM100 and AM200.

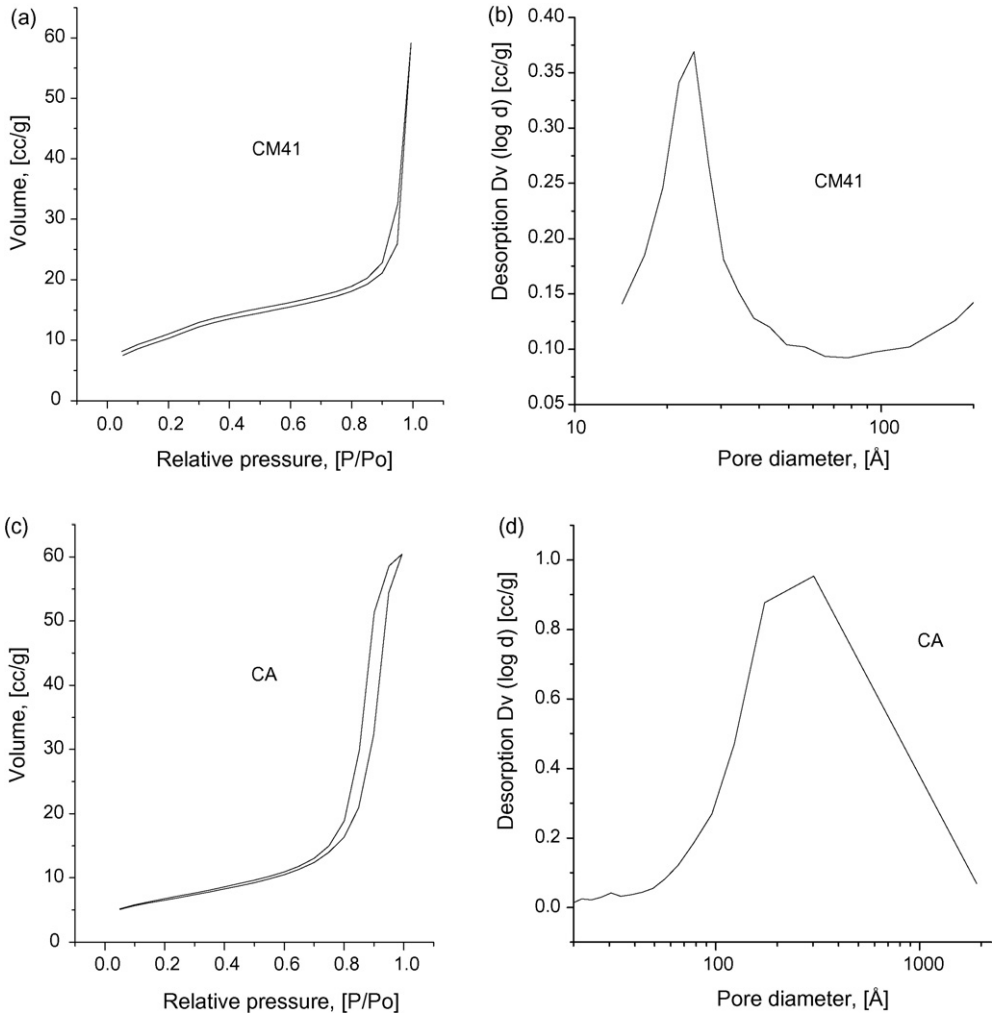

Fig. 9. Isotherms of adsorption–desorption of catalysts: (a) CM 41 and (c) CA and pore size distribution of catalysts: (b) CM 41 and (d) CA.

460 cm^{-1}. The changes of frequency can be explained in terms of the modification of the bond of oxygen atoms and width of stretching band was derived from the sum of a statistical distribution and centered on an average value. The band in the range of 1247–1052 cm^{-1} corresponded to the asymmetric stretching vibration mode of bond Si–O–Si. The bands defined at 581 and 473 cm^{-1} can be attributed to a tetrahedral bending of the Si–O bond with a knocking effect of the molecules.

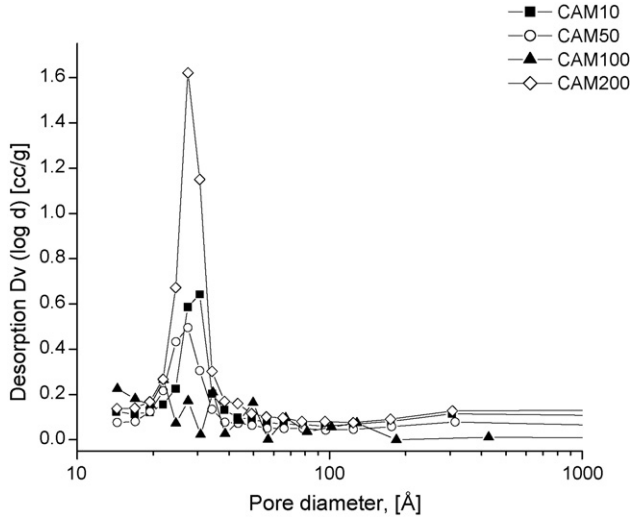

Fig. 10. Pore size distribution of catalysts: CAM10, CAM50, CAM100 and CAM200.

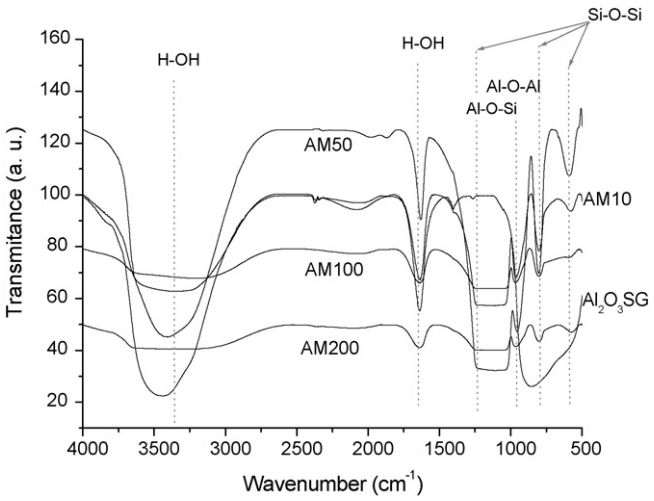

Fig. 11. FTIR spectra of the Al_2O_3–MCM-41 supports.

Finally, the band in the region of 805 cm^{-1} corresponded to a symmetrical stretching of the Si–OH bond [16].

3.4. Hydrothermal stability of Al_2O_3–MCM-41 supports

Similarly to previous studies [17], the structural stability of MCM-41 and its Al_2O_3 modified material were estimated for their hexagonal array by using hydrothermal treatment at exaggerated experimental conditions in presence of water steam, the low angle X-ray diffraction patterns of treated samples are shown in Figs. 12–14. The XRD results indicated that the pure MCM-41 has relatively lower stability than that of its modified analogues. These results slightly affected the intensity of the solid but the pore structure remain intact particularly at high Si/Al ratio (AM200), while AM100 as well as AM50 showed decreasing intensity ($d_{1\,0\,0}$) with increasing the streaming temperature as shown in Figs. 13 and 14. Nevertheless, XRD results indicated that the porous structure withstand up to about 873 K under 100% water steam. This property might result from significant differences in hydrolysis rates of the –O–Al–O– and –O–Al–O–Si–O bonds with respect to –O–Si–O bonds. Therefore, the increase of the thermal resistance for the series (Al_2O_3–MCM-41) was verified, which

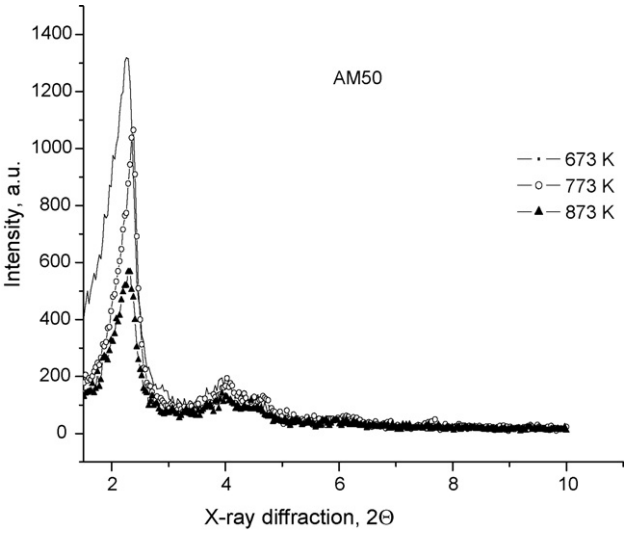

Fig. 13. XRD patterns of the calcined samples: AM50 after treatment at $T = 673$, 773 and 873 K with 100% water steam.

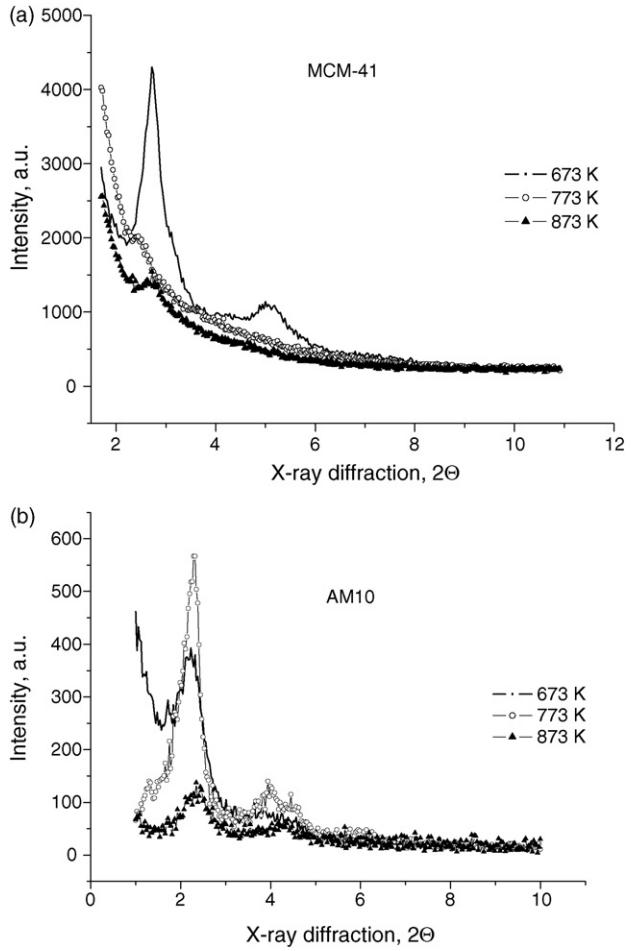

Fig. 12. XRD patterns of the calcined samples: (a) MCM-41 and (b) AM10 after treatment at $T = 673$, 773 and 873 K with 100% water steam.

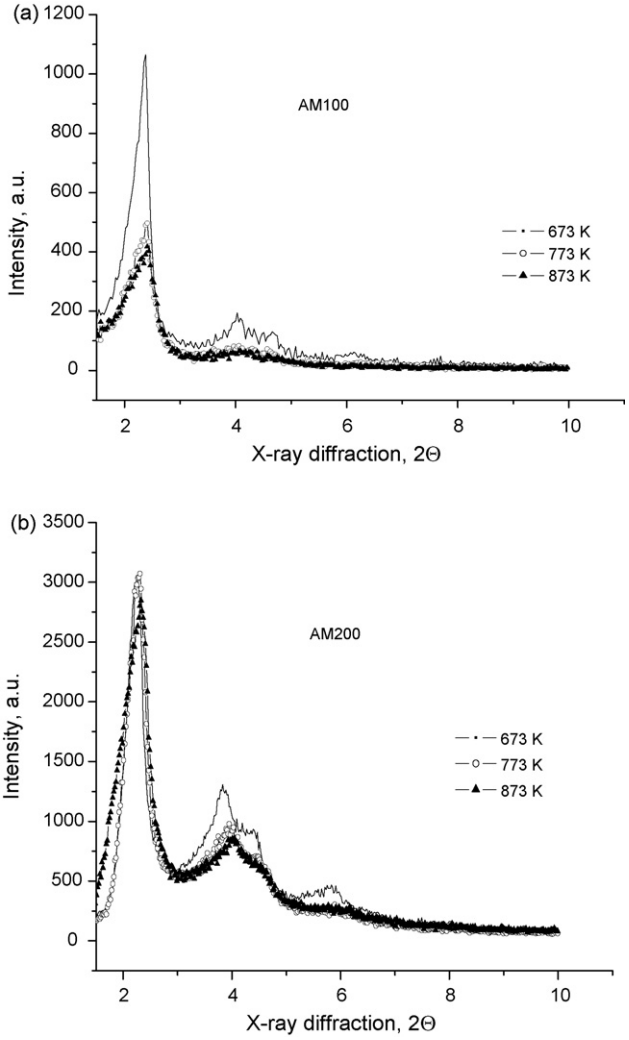

Fig. 14. XRD patterns of the calcined samples: (a) AM100 and (b) AM200 after treatment at $T = 673$, 773 and 873 K with 100% water steam.

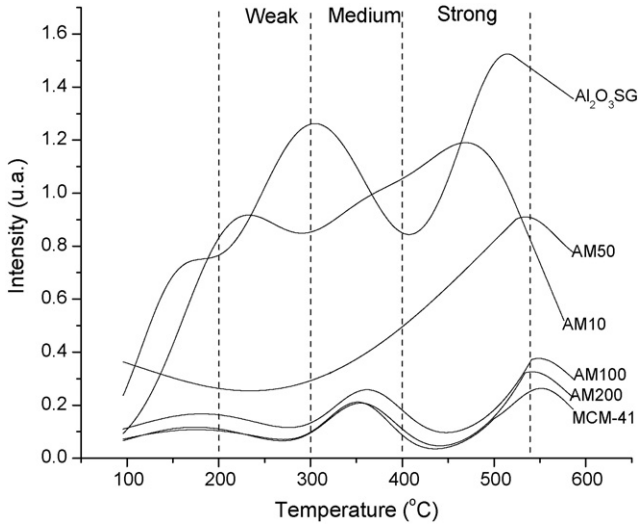

Fig. 15. Ammonia temperature programmed desorption (TPD) thermograms of supports.

increases the potential applications of these materials under severe hydrotreating reaction conditions.

3.5. Surface acidity of Al_2O_3–MCM-41

Generally, MCM-41 support presented the lowest amount of acid sites. As the amount of alumina increased in the Al_2O_3–MCM-41 supports (that means, a decrease in the Si/Al ratio) the surface acidity increases (Fig. 15). The principal objective of this work is to increase the stability as well as acidity of the support by adding alumina, which play a vital role to the hydrodesulfurization and product selectivity during hydrotreating. In this respect, the alumina containing MCM-41 support showed the highest acid character, but it varies with the composition of alumina added into the MCM-41 as shown in Table 5. The quantitative evaluation of acid sites observed in Table 5 indicates that the total number of acid sites in the Al_2O_3–MCM-41 supports is relatively higher than MCM-41. The surface density of acid sites of the Al_2O_3–MCM-41 supports tends to increase with Al loading up to Si/Al = 10, indicating the better interaction of alumina into the siliceous. With further increase in the Al content acidity is decreasing and this behavior is observed for all types of acid sites. However, this increase is not proportional to Al content.

Fig. 16 presents the profiles of the acid sites distribution for the NiMo supported catalysts (NiMo/Al_2O_3–MCM-41) along with CM41 and CA. The acidy does not vary significantly with variation of alumina content, that is CAM(x) where x (Si/Al) = 10, 50, 100 and 200. In the region of population of low temperature (473–573 K) acid sites indicate that most of the acid strength is weak and it follows the order: CAM10 > CAM50 > CAM100 > CAM200 as shown in Table 5.

3.6. Activity test

The supported NiMo catalysts were tested for DBT hydrodesulfurization in a batch reactor, the reaction products obtained for sulfided NiMo/Al_2O_3–MCM-41 catalyst were biphenyl (BP) produced by direct desulfurization or the hydrogenolysis (HYG) route, and cyclohexylbenzene (CHB) produced by the hydrogenation (HYD) route. The reaction paths of hydrogenolysis and hydrogenation are shown in Fig. 1. During the reaction decalin (solvent) showed slight interconversion *cis* to *trans*, while decane (internal standard) remained unconverted at the end of the reaction. The analyses of products were carried out each 30 min by using on-line sampling port and the decane was used to perform the mass balance of the reaction. Negligible amounts of tetrahydrodibenzothiophene and dicyclohexylbenzene were detected in between the reaction as well as after 3 h time-on-stream. The DBT conversion as well as BP and CHB selectivities with variation of support composition are reported in Table 6 and Fig. 17. It appears from these activity results that the reaction is affected by the textural as well as the acidity of the catalysts. A

Table 5
Surface acidity of the supports and catalysts determined by NH_3 TPD

Samples	Specific acidity (μmol NH_3/m^2)	Acidity (μmol NH_3/g)			
		Total acidity	Distribution of acid sites (K)		
			Weak, 473–573	Medium, 573–673	Strong, 673–713
Supports					
MCM-41	0.115	115	17	33	65
AM10	1.001	982	253	273	456
AM50	0.412	512	54	150	308
AM100	0.158	144	23	19	102
AM200	0.15	159	22	66	71
Al_2O_3 SG	3.8	820	145	285	390
NiMo catalysts					
CA	6.44	973	396	319	258
CM41	5.09	1234	637	333	264
CAM10	10.11	2236	684	755	787
CAM50	4.22	837	308	258	271
CAM100	9.2	1454	658	371	425
CAM200	3.71	1306	698	362	246

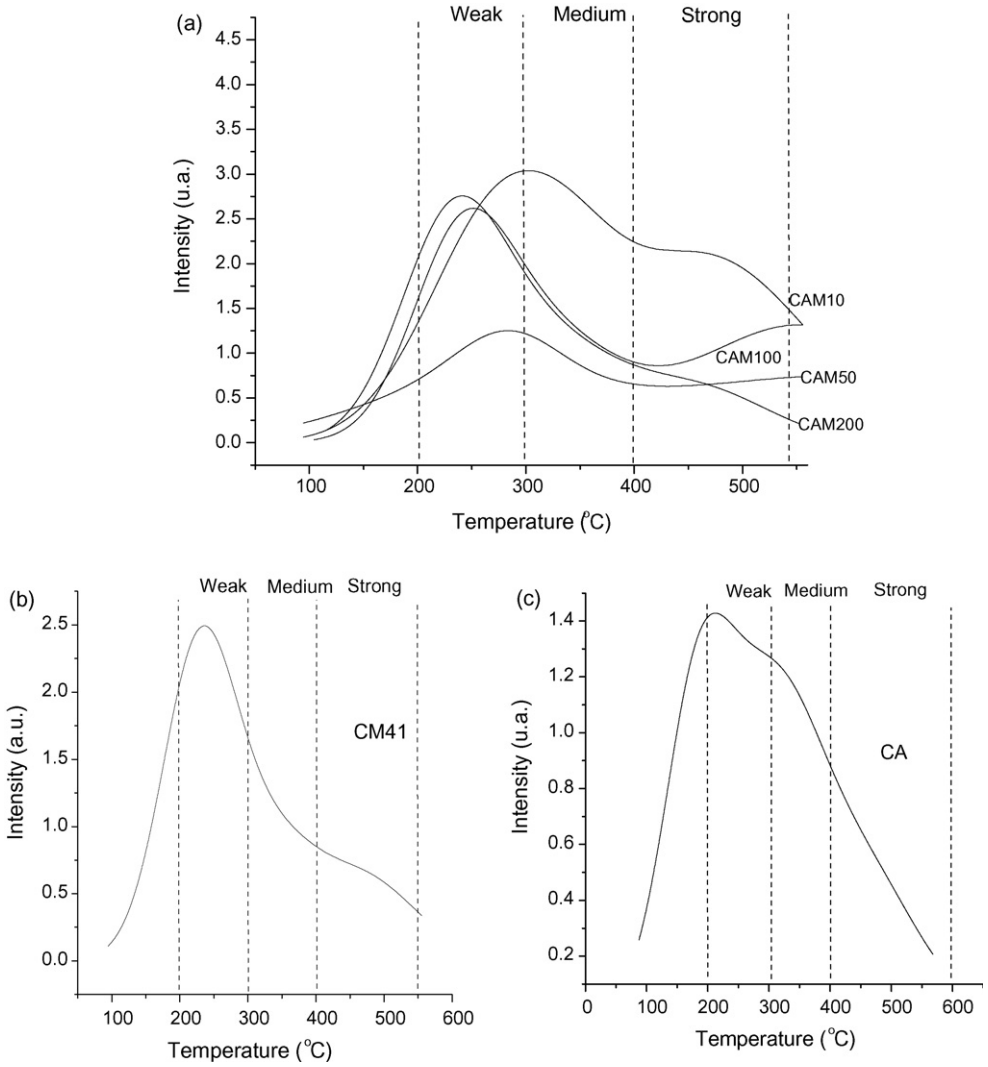

Fig. 16. Ammonia TPD thermograms of catalysts: (a) CAM10, CAM50, CAM100, CAM200, (b) CM41 and (c) CA.

maximum of catalytic activity was reached at a Si/Al ratio of 10 of the support composition. However, for higher Si/Al ratio the activity remains lower due the low dispersion of alumina and thus the lower number of catalytic (NiMoS) sites.

The product selectivity is mainly oriented to the composition of support and acidity variation, suggesting a major promotional on the hydrogenation route. In Table 6 the value obtained for pure MCM-41 (CM41) was about 20% lower in comparison

Table 6
Catalysts hydrodesulfurization activities and its product selectivity

Catalysts	DBT conversion (%)	Selectivity		
		BP	CHB	BP/CHB
CAM10	50	28	22	1.31
CAM50	37	29	8	3.68
CAM100	28	25	3	7.37
CAM200	31	26	5	4.93
CM41	30	24	6	3.94

$T = 613$ K; $P = 45$ bar.

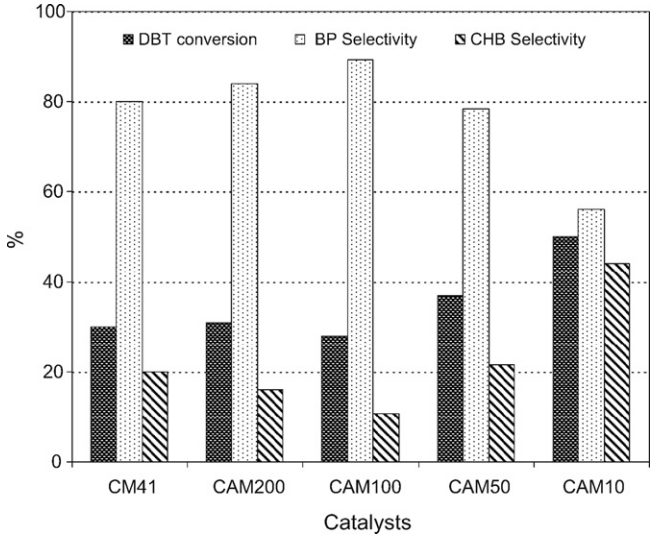

Fig. 17. DBT hydrodesulfurization conversion and product selectivity with $NiMo/Al_2O_3$–MCM-41 catalysts.

with the catalyst having a Si/Al of 10 (CAM10). Generally, all the CAM catalysts presented high selectivity toward biphenyl, because they were able to take the direct hydrodesulfurization way carrying out the C–S ring cleavage of dibenzothiophene. Since CAM10 catalyst has relatively high acidity, it could hydrogenate one of the aromatic rings before hydrogenolysis and hence a higher amount of cyclohexylbenzene is produced [13]. Thus, the activity properties of materials were a consequence of alumina content in the samples, due to the increment of acidity properties.

4. Conclusions

The sol–gel incorporation method of Al_2O_3 to the structure of the MCM-41 did not produce any major changes in the characteristic of hexagonal arrangement of meso-porous materials. Therefore the sol–gel method allows for the modification of the wall-thickness and textural properties of the solid during the synthesis conditions.

The XRD characterization of the Al_2O_3–MCM (AM) showed that MCM-41 and γ-Al_2O_3 were present, indicating the presence of both materials in the synthesized solids. For the supports with Si/Al ratios >50 the diffraction angles in $d_{1\,0\,0}$ and $d_{2\,0\,0}$ presented a better definition of their crystallinity, since small quantities of alumina allowed the empty spaces inside the mesopores to be occupied in a uniform way. The acidity of the supports and catalysts increased considerably as the alumina content was increased in the supports and catalysts except for AM50 and CAM50.

The Al_2O_3–MCM-41 supports produced a decrease of the surface area between 67 and 81%, which can be attributed to the stability of the siliceous material. Higher amount of alumina in the CAM10 catalyst promotes the reaction toward hydrogenated products of DBT indicated by high concentrations of CHB, which is attributed to a promoted acidity of the catalysts.

Acknowledgements

This work was performed with the financial support of COSNET 595.02-P. The authors are thankful to Victor Lara for the XRD measurements.

References

[1] K.G. Knudsend, B.H. Cooper, H. Topsφe, Appl. Catal. 189 (1999) 205–215.
[2] R.L. Dickenson, A.D. Karp, H.E. Johnson, Fourth Forum on Advances in the Refining Industry–Pemex Refinación and Instituto Mexicano del Petróleo, 1998, p. 18.
[3] J. Beck, J. Vartuli, W. Roth, M. Leonowicz, C. Kresge, K. Schmitt, C. Chu, D. Olson, E. Sheppard, S. McCullen, J. Higgins, J. Schlenker, J. Am. Chem. Soc. 114 (1992) 10834–10843.
[4] C.T. Kresge, M.E. Leonowicz, W.J. Roth, J.C. Vartuli, J.S. Beck, Nature 359 (1992) 710.
[5] J.M. Domínguez, E. Terrés, A. Vázquez, Micropor. Mesopor. Mater. 66 (2003) 341–348.
[6] A. Vazquez, T. Lopez, R. Gome, X. Bokhimi, J. Mol. Catal. 167 (2001) 91–99.
[7] Y. Lee, Catal. Today 38 (1997) 213–219.
[8] D.S. Maciver, H.H. Tobin, R.T. Barth, J. Catal. 2 (1963) 485.
[9] U.A. Sedran, N.S. Fogoli, Appl. Catal. 19 (1985) 317.
[10] U. Cielsa, F. Schüth, Micropor. Mesopor. Mater. 27 (1999) 131–149.
[11] M. Houalla, N.K. Nag, A.V. Sapre, D.H. Broderick, B.C. Gates, AIChE J. 24 (1978) 1015–1021.
[12] K.-C. Park, D.-J. Yim, S.-K. Ihm, Catal. Today 74 (2002) 281–290.
[13] T. Klimova, M. Calderón, J. Ramírez, Appl. Catal. A: Gen. 240 (2003) 29–40.
[14] J. Ramírez, R. Contreras, P. Castillo, T. Klimova, R. Zarate, R. Luna, Appl. Catal. A: Gen. 197 (2000) 69–78.
[15] G. Leofanti, M. Padovan, G. Tozzola, Catal. Today 41 (1998) 207–219.
[16] X.-S. Wang, X.-W. Guo, Catal. Today 51 (1999) 177–186.
[17] R. Silva-Rodrigo, C. Calderon-Salas, J.A. Melo-Banda, J.M. Domínguez, A. Vazquez-Rodríguez, Catal. Today 98 (2004) 123–129.